

Multi-Omic analysis

Elucidating Amphotericin B resistance in *L. mexicana* promastigotes using a Multi-Omics approach

2117832¹

¹University of Glasgow, Glasgow, G12 8QQ, Scotland

Associate Editor: XXX

Received on XXX; revised on XXX; accepted on XXX

Abstract

Motivation: Leishmaniasis is a neglected tropical disease that affects millions of people across the globe. A repurposed anti-fungal drug, Amphotericin B, is being increasingly used to treat for Leishmaniasis. Recently, there have been increasing reports of drug-resistant strains emerging and causing a re-emerging healthcare crisis. In this report, we used a multi-omic approach to determine the mechanisms of Amphotericin B resistance on the genomic, metabolic, and proteomic levels.

Results: Our genomic results show that missense mutation in the enzyme sterol 14- α demethylase, an essential enzyme in the ergosterol pathway. Other SNPs were also identified and have been linked to drug-resistance and the sphingolipid pathway. In our metabolomics results, we found evidence of sterol 14- α demethylase products accumulating in our drug-resistant lines and leading us to believe that the missense mutation, that isn't in the enzymes' active site, is somehow causing a disruption to the ergosterol pathway. This led us to conduct a series of *in silico* experiments, such as substrate docking, molecular dynamics, and protein – protein interaction simulations to determine the impact of the mutation. We didn't find any differences in substrate docking between wildtype and mutant enzyme, this corroborates our metabolomics findings that the enzyme is still active. The molecular dynamics results shows that the mutant enzyme is less compact, and that this has caused disassociation with the partner enzyme, sterol reductase. This report shows the benefits of using a multi-omic approach to gain both a deep and broad insight into the biomechanisms of drug resistance and highlights the importance of drug-resistance research.

Availability:

Contact:

Supplementary information:

1 Introduction

Leishmaniasis is caused by *Leishmania spp.*, a protozoan parasite transmitted by sandflies in its promastigote form. It evades the human immune system by integrating into macrophages as an amastigote. It has two main clinical forms: visceral, which can cause deadly damage to internal organs, and cutaneous, which causes disfiguring topical lesions. Being endemic to poorer regions and having a complex lifecycle, treatments for this have been either too costly or toxic, hindering effective

administration.

Recently, Amphotericin B (AmpB), a polyamine drug that was initially used against fungal diseases, has become one of the leading treatments of Leishmania. Previously, AmpB was an expensive treatment, but the Gilead pharmaceutical company has been giving away the treatment to help lower the burden of disease in endemic countries. The reason that the treatment could be adapted to Leishmania, is because both *Leishmania spp* and fungi use ergosterol as the main sterol for their cell membranes (Cavassini et al., 2021; Barrett and Croft, 2012). The mode of action of AmpB hasn't been fully elucidated but evidence shows that numerous AmpB molecules sit

within the phospholipid bilayer and creates a pore to cause an efflux of the inner cytoplasm (Ramos et al., 1996).

The wide-spread adoption of next-generation sequencing techniques has allowed researchers to perform genome-wide sequencing at affordable costs and has allowed them to build reference genomes. These reference genomes are crucial in comparative genomics of resistant line genomes against the “wild type” reference. The generation of parallel *in vitro* resistant cell lines allows us to find common mutation hotspots. These have been done to determine resistant genomic markers in Trypanosomes, Leishmania and Plamodium (Graf et al., 2016; Coelho et al. 2012; Cerqueira et al., 2017).

Metabolomics allows us to quantify and identify an organisms’ molecular signals that are the product of complex interactions between genome and proteome through mass spectroscopy. The experimental design is similar to the comparative genomic studies from before, where we use cell extracts instead of DNA. The data allows us to compare changes in metabolic pathways caused by the presence of the drug. Due to the untargeted nature of mass spectroscopy studies, we can have greater insight into the mode of action of the drug and/or any compensatory metabolite regulation that increases organism survival (Vincent and Barret, 2015). A study conducted by Berg et al. (2015), generated multiple *Leishmania* spp. cell lines resistant to single or combinatory treatments. Cell extracts underwent a Liquid chromatography and mass spectrometry (LC-MS) analysis with the signals being identified with a Leishmania specific metabolome database. This allowed them to determine differences in metabolite profiles of both proline and lipid pathways.

The priorly discussed comparative genomics allows us to identify mutations that occur in protein coding genes. The mutations can lead to structural changes in the protein that alter active sites and protein conformation that confers resistance. The effect of these alterations can be studied through protein modelling and virtual ligand/substrate docking simulations.

Ergosterol is the target molecule of AmpB, as stated earlier, and this is accounts for 70% of the sterols found in *L. mexicana*. A complex 11 step pathway is required alter lanosterol to ergosterol, with many of these reactions taking place in the endoplasmic reticulum. *Leishmania* spp. are auxotrophic for cholesterol and harvests it from its environment and incorporates it into the plasma membrane, and accounts for 15 – 28 % of sterols (Goad et al., 1984; Yao and Wilson, 2016). There has been some characterisation of the multi-enzyme complex of ergosterol biosynthesis proteins that occurs in *S. cerevisiae* (Mo and Bard, 2005; Mo, Valachovic, and Bard, 2004). This is relevant as *Leishmania* spp. may have a comparable complex, although it hasn’t yet been characterised. If properly understood, this could represent a novel target for future treatments.

In this paper, we will use a multi-omics approach of genomic, metabolomics, and proteomics to elucidate the mechanisms of AmpB resistance in *L. mexicana*. We will discuss the effect of a missense mutation on an ergosterol pathway enzyme, and the perturbations caused to ergosterol biosynthesis in the AmpB resistant (AR) lines.

2 Methods

2.1 Cell lines

L. mexicana cell lines were developed in accordance with methods used in Mwenechanya et al. (2017). Strain MNYC/BZ/62/M379 were exposed

Name	Version	Link / Reference
Trim Galore	0.6.6	https://github.com/FelixKrueger/TrimGalore
Bowtie 2	2.4.3	https://bowtie-bio.sourceforge.net/bowtie2/index.shtml
Freebayes	1.3.6	https://github.com/ekg/freebayes
VCFfilter	1.0.3	https://github.com/vcflib/vcflib#vcffilter
Variant Tool Chest (VTC)	1.0	https://github.com/mebbert/VariantToolChest
SnpEff	5.0e	https://pcingola.github.io/SnpEff/se_introduction/
SnpSift	4.3t	https://pcingola.github.io/SnpEff/ss_introduction/
Integrative genome viewer (IGV)	2.16.1	Robinson, J.T., Thorvaldsdóttir H., Winckler W., Guttman M., Lander ES, Getz G, and Mesirov JP (2011). Integrative genomics viewer. <i>Nat. Biotechnol.</i> , 29, pp.24-26.
PIMP	1.0	http://polyomics.mvls.gla.ac.uk/
MetaboAnalyst	5.0	https://www.metaboanalyst.ca/
SignalP	5.0	https://services.healthtech.dtu.dk/services/SignalP-5.0/
AlphaFold	1.5.2	Mirdita, M., Schütze, K., Moriaki, Y., Heo, L., Ovchinnikov, S. and Steinegger, M., 2022. ColabFold: making protein folding accessible to all. <i>Nature methods</i> , 19(6), pp.679-682.
SWISSMODEL	N/A	swissmodel.expasy.org
SWISSDock	N/A	http://www.swissdock.ch/
SWISS QMean	N/A	https://swissmodel.expasy.org/qmean/
UNRES	29.06.2018	https://unres-server.chem.ug.edu.pl/
ClusPro	2.0	https://cluspro.bu.edu/

Fig. 1. Summary list of Tools and Programs used in the analysis of the data.

to doubling increments of 0.0135 μ M of AmB to a final concentration of 0.27 μ M to develop the AR lines. Strains were cultured in HOMEM + 10% foetal bovine serum media.

2.2 Genome alignment

Genome sequencing of both cell lines were done on the Illumina platform. Illumina reads were quality controlled with Trim Galore with read sections below a Phred64 score of 20 removed. Genome alignment against the reference genome *L. mexicana* MHOM/GT/2001/U1103 was carried out with Bowtie2 using standard flags on the University of Glasgows’ High Performance Computer cluster. Alignment files were sorted using Samtools and both Bam files were merged using bamaddr.

2.3 SNP calling and Effect prediction

Variants were determined using Freebayes, using default flags, and were then piped directly to VCFfilter. VCFfilter was used to remove SNPs with quality scores below 20. Filtered SNPs were put through Variant Tool Chest to select for SNPs unique to the AmpB resistant line using this set operator: c[data[AmpB]:data[WT]]. SnpEff then annotates those SNPs to predict the impact effect of mutations on genes and link them to the transcript they impact. SnpSift was used to filter for moderate to high effects, where missense mutations have moderate effects and stop-gained, frame-shift mutations have high effects. This then outputs the AmpB resistant compliment SNPs to a VCF file, with this format: Chromosome, SNP position, ID, Reference allele, Alt allele, Impact type, Transcript code, Variant in HGVS (DNA) notation, and Variant in HGVS (protein) notation.

2.4 SNP UTR region associator

A custom Python script was written to associate SNPs with putative UTR regions. The script uses the gffutils library to create a database of transcript coordinates. It then iterates through a list of SNP coordinates from the vcf file generated from the SnpEff/Sift tools. The script then checks if the SNP resides within 200bp upstream of the transcript start or 500bp downstream of the transcript end. These UTR lengths were estimated by Dillon et

al. (2015) in *L. major*. It then writes the SNP position in the chromosome and the transcript code it affects to a text file.

2.5 TriTrypDB

TriTrypDB was used to get transcript product descriptions from the transcript codes that are outputted by SnpSift and our custom Python UTR code. A list of product descriptions, transcript position was generated using the search tool : Identify Genes based on List of IDs.

2.6 Metabolomics

Metabolomics data was generated using an LC-MS untargeted metabolomics approach. Four replicate cell extracts per group were taken during their mid-log phase. Then were processed for separation and mass detection using HILIC separation column and Orbitrap Exactive mass spectrometer (Mwenechanya et al., 2017). The metabolomics data was initially processed using Glasgow Polyomics’ PiMP web platform. This enabled us to differentiate and annotate peaks, according to the Metabolomics Standard Initiative, and were mapped to KEGG metabolomic maps. This also calculated log-fold changes, adjusted P-values, and Log odds between our two groups.

Peak m/z ratios for each replicate were then further processed using the MetaboAnalyst web platform. This was done to conduct further statistical analysis of our data. We used their one-factor statistical analysis module, which replaced missing data with 1/5 of the minimum positive values, as some statistical tests can’t handle missing values. Variables that are constant between groups are determined using the interquartile range were filtered to aid compute time and improve statistics; the data was also log-10 normalised. This data was then used to generate volcano plots and peak pattern correlation plots were done, correlation coefficients were calculated using Pearson R test.

2.7 Proteomics

Firstly, we downloaded protein sequences for Sterol 14- α demethylase (CYP51), ACU00618.1, and Sterol reductase (SR), XP_003878080.1. SignalP 5.0 was used to determine the presence of signal peptides in our protein sequences and their cleavage sites. Signal peptides were cleaved in CYP51, and none were found in SR.

To determine the structures of CYP51 and SR, a few protein modelling tools were used to determine the yet to be characterised structure of CYP51 in *L. mexicana* based on the *L. infantum* structure as a template (PDB code: 3L4D). Models were generated using AlphaFold (Mirdita et al., 2022), Swissmodel (Waterhouse et al., 2018), and Phyre2 (Kelley et al., 2015) on their default settings. Models were quality checked using SWISS-Model QMEANDisCo method.

Substrate docking modelling was carried out with SwissDock, where Obtusifolol was used as the substrate in the modelling as it resembles the true substrate 4,4-dimethylcholesta-8,14,24-trien-3 β -ol. These docking simulations were carried out with wildtype (WT) and mutant (MT) models of CYP51 to determine the most energetically favoured position, measured in ΔG (kJ/mol).

Molecular dynamic modelling was carried out using the UNRES server, using the predicted structure of CYP51 (WT or MT) and the most energetically favoured position of the substrate. The modelling was carried out using the default settings.

Protein-protein interaction simulations were carried out with ClusPro. The structure of Sterol reductase (LmxM.31.2320) was determined using

	WT1	WT2	AmpB1	AmpB2
Reads trimmed	11.2 %	17.0 %	11.5 %	16.9 %
Unaligned reads		23.0%		19.0%
Aligned reads 1 or more times		77 %		81 %

Fig. 2. Genomics Statistics for TrimGalore and Bowtie2

AlphaFold, as there was no related and experimentally determined structure on the PDB. Both the WT and MT versions of the structures of CYP51 and SR were used for the interaction simulations on default settings. The first model from the balanced category were used for analysis for both WT and MT versions.

3 Results

3.1 Genomics

Sequencing of the WT and AR lines generated 17.5 million and 15 million paired reads using Illumina GAIx sequencing platform. Once processed by the genomics pipeline outlined in our methods, on average 14% of the reads were quality trimmed before alignment using Bowtie 2 (Figure 2 and 3). Due to the inherent plasticity of the Leishmania genome only an average of 22% of the reads were aligned to reference genome. This plasticity and tendency for the presence of irregular aneuploidy in the genome would explain the lower alignment, seen in Figure 2 (Negreira et al., 2022).

The next step in our pipeline was to visually inspect the aligned BAM files, using IGV, to verify for any large errors that may have occurred during alignment. The BAM files of WT and AR were merged, and SNPs were identified using Freebayes. SNPs were filtered for quality and VTC was used to select for mutations unique to the AR lines. From this 1132 SNPs were found to be unique to the AR lines, of which 61% were either hetero / homozygous for alternative allele, 22% were homozygous for the reference, and 17% had missing call information.

The snpEff / Sift tools were used to allocate SNPs to the transcripts they were affecting and those that had moderate to high impact were selected. Moderate impact SNPs were either missense variants or in frame deletions; and high impact SNPs were either stop gained or frameshift variants. In our case, only missense and stop gained mutations were detected. This gave us shortlist of 134 SNPs, 9 of which were high impact, that affected 89 transcripts. However, 44 of these transcripts were described as conserved hypothetical proteins on the TriTrypDB database.

We will present here the key SNPs within the shortlist that are relevant to drug resistance and the ergosterol pathway. These SNPs have all caused missense mutations in transcripts related to ABC transporters (LmxM.11.1220/ 1240/ 1290), a nucleoporin (LmxM.28.3030), iron transporters (LmxM.30.3060 / 3070), and CYP51 (LmxM.11.1100). Two other transcripts were also affected by missense mutations: Sphingosine kinase (LmxM.26.0710.1) and 5'-AMP-activated protein kinase catalytic subunit alpha (LmxM.08_29.2020.1); that are both involved in the sphingolipid pathway, an alternate structural lipid.

Since UTR regions in Leishmania genomes have yet to be characterised, none of the SNPs could be associated to those regions. Using the custom Python script described in the method, we managed to associate 6% of the SNPs to these putative UTR regions. 63 UTR SNPs

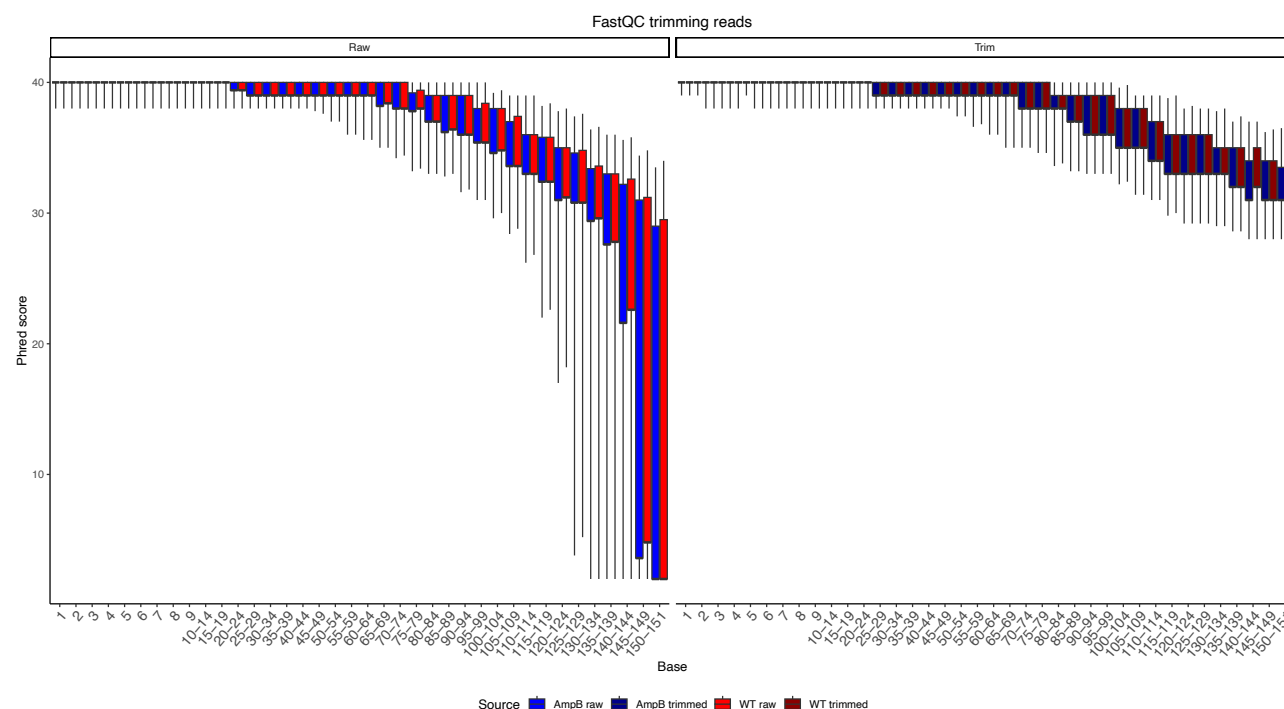


Fig. 3. Figure 1. FastQC of both raw and trimmed paired reads. Phred64 score on the y-axis and base position on the x-axis. Here we can see TrimGalore improved the quality of the 5' end of the paired reads. The average Phred score of both pairs is displayed here.

have potentially affected 42 genes although only two are of interest, Acyl CoA synthetase (LmxM.03.0230) and acetyltransferase (LmxM.03.0130). These two proteins are involved in the fatty acid biosynthesis pathway.

3.2 Metabolomics

We conducted an analysis of LC-MS untargeted metabolomics from cell extracts from our wildtype and AR lines. This generated data on 2811 metabolites from 3144 peaks. However, when comparing the peaks between WT and AR lines, only 369 peaks are found to have significantly different log fold changes (Figure 4). One of the peaks that had the highest log fold change was peak 1051, where low abundance was detected in the WT sample whereas a great relative abundance was detected in AR. PiMP has attributed the peak to 4,4-dimethylcholesta-8,14,24-trien-3 β -ol, the product of CYP51, although other sterols such as coristerol and dehydroconicasterol, were also attributed.

Correlation analysis of peaks were conducted using the PatternHunter function on MetaboAnalyst, the correlation distance was calculated using Pearson r correlation (Figure 5). When running a correlation analysis of peak 1051, we find that peak 701 is highly correlated. It has an m/z ratio of 395.4, which could represent a dehydrated form of peak 1051, since that is the m/z difference of H₂O (18 m/z). Peak 2031 is another related peak, with a m/z of 387. This peak could represent cholesterol as it has the same atomic weight; however, many peaks in our data are near that m/z ratio. Finally, Peak 705 (454 m/z) was also correlated and was annotated as stigmasterol as well as other sterols.

The next set of peaks we will present are those that have a lower relative abundance compared to WT lines. Peaks 451, 502 show a lower relative abundance, with other related peaks, being annotated as Ceramides and Glycerophosphocholine. These along with Peaks 516 and 1692, that have a higher relative abundance to WT, all belong to the sphingolipid

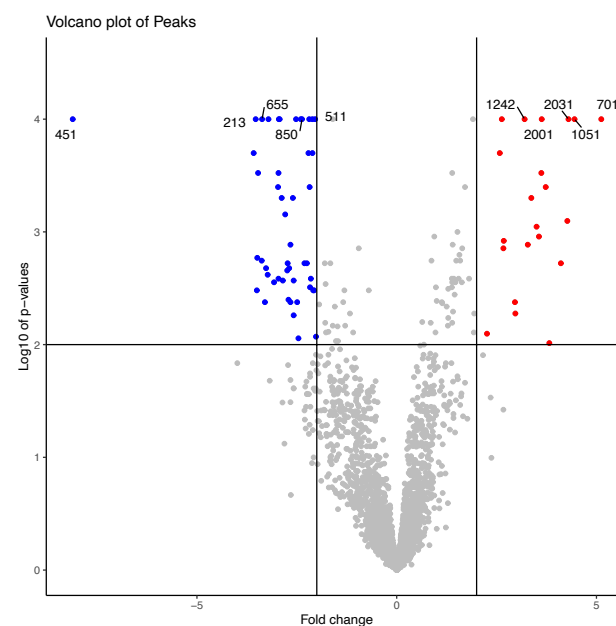


Fig. 4. A volcano plot of LC-MS peak log-fold changes against log-10 transformed P-values. Upregulated peaks are highlighted in red, downregulated peaks are highlighted in blue, and non-significant peaks are left in grey. Significant peaks have a log-fold change > 2 and an adjusted P-value < 0.01.

biosynthesis pathway (Zhang and Beverley, 2009). Peak 516 was identified as ethanolamine phosphate and 1692 was annotated as CDP-choline. Peak 1902 was annotated as hexose-phosphates which were lower in AR lines by 3-fold changes. All the peaks presented here can be found in Figure 6,

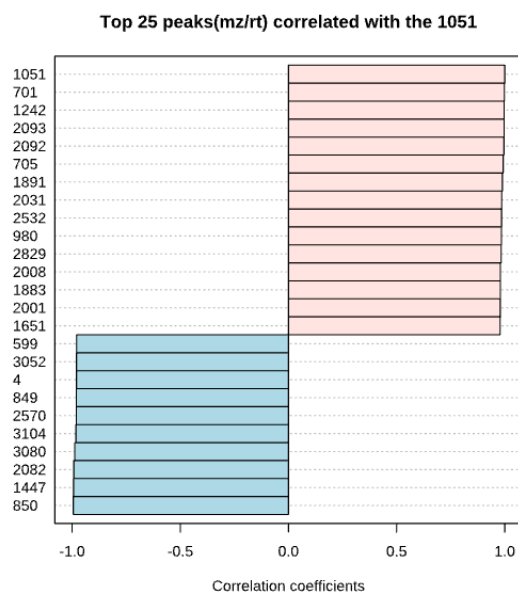


Fig. 5. Pattern Hunter peak correlation table of 1051. This shows the LC-MS peaks that are closely correlated profiles to 1051 in red, using a Pearson R correlation test. In blue are peaks that have uncorrelated profiles to peak 1051.

Peaks of Interest				
Possible metabolites	Peak id	Log FC	Adjusted P-value	Log Odds
4,4-dimethylcholesta-8,14,24-trien-3 β -ol	1051	4.45	0.00	13.72
Dehydrated sterol	701	5.12	0.00	12.64
Ceramide	451	-8.11	0.00	11.96
Cholesterol	2031	4.30	0.00	8.36
Ergosterol	655	-3.37	1.00 \times 10 $^{-4}$	6.66
Hexitose-phosphates	1902	-3.58	2.00 \times 10 $^{-4}$	5.90
Stigmasterol	705	2.58	2.00 \times 10 $^{-4}$	5.82
Ethanolamine phosphate	516	3.56	1.10 \times 10 $^{-3}$	3.61
Glycerophosphocholine	502	-3.38	1.80 \times 10 $^{-3}$	2.76
CDP-choline	1692	1.93	7.80 \times 10 $^{-3}$	0.31

Fig. 6. Summary table of peaks of interest.

with possible metabolite annotations, p.adjusted values, Log-fold changes, and Log Odds.

3.3 Structural Proteomics

Next, we decided to model the point mutation found in CYP51 to determine its effect on the structure and ligand binding affinity. Since there is no structure for CYP51 from *L. mexicana* on the PDB, we had to use model prediction using the structure from *L. infantum* as a template. *L. infantum* was used as the template because the Smith-Waterman protein alignment showed a 97 % identity and 99 % similarity. Prior to predicting the models, we checked for signal peptide cleavage sites in the sequence using SignalP. We decided to trim the protein sequence at the position 23 cleavage site peak.

Here we used AlphaFold, Swissmodel, and Phyre2 to model monomers of both the WT and MT CYP51 structures. These were compared against each other to verify for any errors, seen in Figure 7. We can see that the

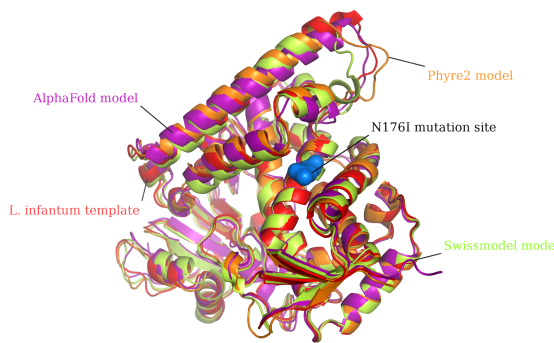


Fig. 7. CYP51 protein modelling comparison. Here we have the *L. infantum* template (red), AlphaFold (purple), Phyre2 (orange), and Swissmodel (green) CYP51 models all superimposed. This superimposition and annotations were done in PyMol.

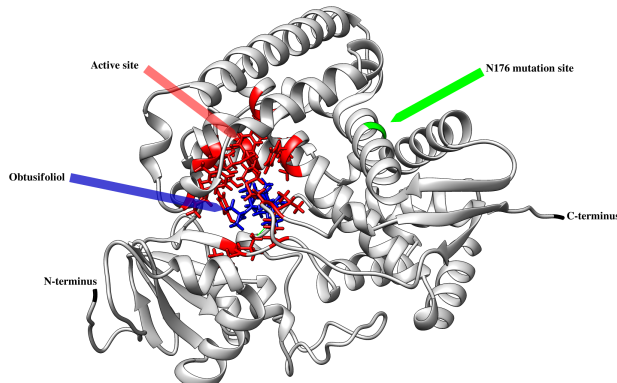


Fig. 8. Substrate docking of CYP51 with 14 alpha-dimethyl-5 alpha-ergosta-8,24(28)-dien-3 β -ol. The active site of the enzyme is highlighted in red, ligand in blue, and the N176I mutation in green. The distance between the closest residue in the active site and N176I was calculated to be 15 Angstroms. Annotations were done in PyMol.

models align to the template, with the main differences coming from the loop structures. We chose the AlphaFold model for later analyses although all models had an QMEANDisCo model quality score of 0.81 ± 0.05 .

We then ran molecular docking simulations with the enzyme ligand, 14 α -dimethyl-5 α -ergosta-8,24(28)-dien-3 β -ol, using both the WT and MT AlphaFold models on SWISSDock. We chose the simulated ligand position that had the lowest ΔG (Gibbs free energy), indicating the difference in thermodynamic states caused by ligand binding. This represents the binding site that is most energetically favourable.

We then used this docking position in the molecular dynamics' simulation using the UNRES server, this was done to detect changes in protein conformation and flexibility. In Figure 9.a), we can see that there is a difference in the radius of gyration between the WT and MT. Radius of gyration is a measure of the compactness of a protein, where the smaller the radius the more compact the protein. As the simulation runs, we see that the radius of gyration is significantly different and larger in the MT compared to the WT; showing that the MT is less compact. The difference in potential energies between two proteins were significantly different, where the MT has a lower potential energy (Figure 9.b). The potential energy in the simulation is like ΔG and shows the lowest energy at 300 K; this represents the most likely shape of the protein at that temperature.

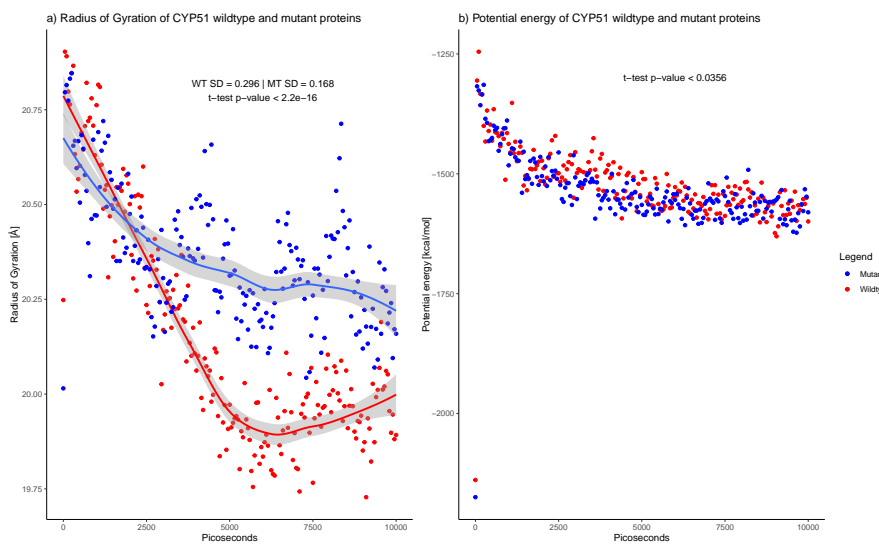


Fig. 9. Molecular dynamic statistics from UNRES. a) Radius of Gyration (\AA) of both WT and MT CYP51 over Time (picoseconds). b) Potential energy (kcal/mol) of both WT and MT CYP51 over Time (picoseconds). Trendlines were estimated using Local Polynomial Regression Fitting, T-tests were used to determine significance, and variation was determined by standard deviation. Mutant protein data points coloured in blue, wildtype in red.

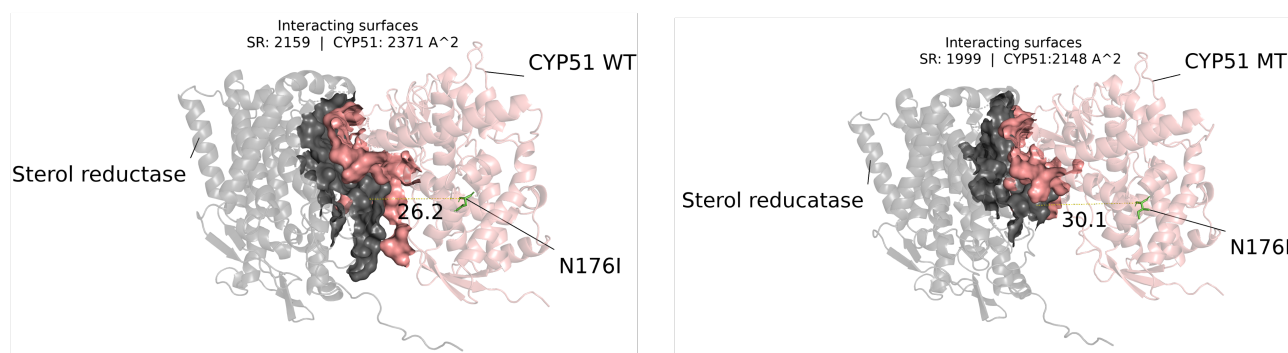


Fig. 10. CYP51 and Sterol reductase protein-protein interaction. Here we have the top balanced interaction model from ClusPro using both the WT and MT CYP51 and the AlphaFold model of SR. On the left, WT CYP51 interacting with SR with interaction surfaces highlighted along with N176I mutation point (green) and on the right, MT CYP51. The distance between the mutation point and closest residue in SR, Valine 188 is also shown. Interaction surfaces and residue distances were calculated using Pymol.

(Liwo et al., 2007).

The final analysis was the protein – protein interaction between CYP51 and SR using Cluspro. We wanted to determine any difference in their interaction and binding affinities caused by the mutation. In Figure 10., we see the top balanced interaction model, where it balances between hydrophobic and electrostatic interactions, for both WT and MT CYP51. We can see the interacting surfaces highlighted with their calculated surface area labelled above. We can also see the distance between the mutation and the closest amino acid in SR (Valine 188). There is an approximate 9% decrease in the interacting surface between both proteins with the MT CYP51, as well as a greater distance (4 \AA) between the proteins towards the N-terminus of CYP51.

4 Discussion

We will begin our discussion with the main candidate that accounts for the resistance seen in the AR lines. From our genomics results, we identified a single missense mutation, asparagine to isoleucine at position 176 (N176I),

in the CYP51 enzyme.

In our metabolomics results, we see that the activity of the enzyme is not affected by this mutation since we can observe its product, Peak 1051 and 701, however the rest of the ergosterol pathway appears to be disrupted, as seen in the -3.4 fold change of peak 655. Due to the limitations of HILIC LC-MS, certain metabolites have co-eluted at the same time and has made it difficult to separate some peaks. However, we can be confident that Peaks 1051 and 701 are products of CYP51 due to their m/z ratios and the fact they have accumulated in AR lines and only have minimal traces in the WT lines.

In protein structure results, we see that the mutation is far from the active site, ~ 15 \AA (Figure 8), and resides in the proximal N terminus. Our molecular dynamics shows us that the MT CYP51 has a less compact conformation and has increased flexibility; this corroborates findings by Vijayakumar and Das, 2018. This led to us to investigate the protein-protein interaction between CYP51 and subsequent enzyme, SR. Using the modelling software ClusPro, it predicted possible surface interactions between the two. Our modelling showed us that there appears to be some

disassociation caused by the mutation, even though the mutation isn't within these predicted interaction surfaces in our models (Figure 10). This would imply that the increased flexibility of the MT CYP51 causes lower binding affinity to SR. A caveat should be made here, as powerful as these *in silico* experiments are, CYP51 and SR structures came from protein modelling algorithms. These interactions are predictions based on predictions, to be truly confident in our results, we would need to determine the real structure of both these proteins with x-crystallography experiments. We could use Co-immunoprecipitation using antibodies to extract the protein complexes and then use Cryo-Em to determine their structure; a protocol can be adapted from Cooney et al. (2023).

The concept of the ergosome that has been characterised by Mo and Bard (2005) where enzymes involved in ergosterol pathway form a central enzyme complex. Since both *S. cerevisiae* and *Leishmania spp.* use this pathway extensively, it is possible that an ergosome is present in *Leishmania spp.* This core of enzymes includes CYP51 and SR and the core is attached to the ER by a scaffolding protein. There is evidence that this mutation could be causing a disassociation of this complex by either causing lowered binding affinity with its partners or perhaps the scaffold protein. However, the ergosome has yet to be fully characterised in *Leishmania spp.* and it would require an *in vitro* or *in silico* experiment of multiple protein – protein interactions to determine the effect of the N176I mutation.

Another potential set of SNPs could be contributing to the resistance, are the ones affecting the two enzymes in the sphingolipid pathway shown in the genomics section. Evidence of changes in this pathway can be seen in Figure 6., where Ceramide / Glycerophosphocholine have decreased in abundance and Ethanolamine phosphate / CDP-choline have increased. This suggests that AR lines are using ceramides to potentially produce either phosphatidylcholines (PC) or phosphatidylethanolamines (PE). The increased prevalence of both PCs and PEs in drug-resistant lines have been found before (t'Kindt et al., 2010; Gutierrez Guarnizo et al., 2021). Both papers have found that these phospholipids contribute to drug resistance by helping *Leishmania spp.* to deal with oxidative stress caused by damage to the mitochondrial membrane. Gutierrez Guarnizo et al. (2021), suggest that PC hydrolysis increases the availability of methyl donor groups that aid against reactive oxygen species. Lastly, there appears to be increased glucose consumption in AR lines (Figure 6), a similar response was found in a CYP51 KO experiment done by Mukherjee et al., 2020. They hypothesise that these KOs cause a switch to the glycolysis pathway for energy consumption and to reduce the generation of reactive oxygen species.

In this report we have shown that a multi-omic approach has the potential to generate corroborating evidence from different disciplines that points to the cause of drug resistance in our AR lines. This has also shown the downsides of using a single drug in targeting a complex protozoan, perhaps using a synergistic combination of drugs that target complimentary pathways could vastly decrease the chances of developing drug resistance. This synergistic combinaation could be determined using a future multi-omic experiment. The multi-omic approach used here could help researchers better understand the mechanisms of drug-resistance not only in *Leishmania* but other pathogens that are constantly developing drug-resistances.

5 References

- Barrett, M.P. and Croft, S.L., 2012. Management of trypanosomiasis and leishmaniasis. British medical bulletin, 104(1), pp.175-196.
- Berg, M., García-Hernández, R., Cuypers, B., Vanaerschot, M., Manzano, J.I., Poveda, J.A., Ferragut, J.A., Castany, S., Dujardin, J.C. and Gamarro, F., 2015. Experimental resistance to drug combinations in *Leishmania donovani*: metabolic and phenotypic adaptations. Antimicrobial agents and chemotherapy, 59(4), pp.2242-2255.
- Cavassin, F.B., Baú-Carneiro, J.L., Vilas-Boas, R.R. and Queiroz-Telles, F., 2021. Sixty years of amphotericin B: an overview of the main antifungal agent used to treat invasive fungal infections. Infectious Diseases and Therapy, 10, pp.115-147.
- Cerqueira, G.C., Cheeseman, I.H., Schaffner, S.F., Nair, S., McDew-White, M., Phylo, A.P., Ashley, E.A., Melnikov, A., Rogov, P., Birren, B.W. and Nosten, F., 2017. Longitudinal genomic surveillance of *Plasmodium falciparum* malaria parasites reveals complex genomic architecture of emerging artemisinin resistance. Genome biology, 18, pp.1-13.
- Coelho, A.C., Boisvert, S., Mukherjee, A., Leprohon, P., Corbeil, J. and Ouellette, M., 2012. Multiple mutations in heterogeneous miltefosine-resistant *Leishmania* major population as determined by whole genome sequencing. PLoS neglected tropical diseases, 6(2), p.e1512.
- Cooney, I., Mack, D.C., Ferrell, A.J., Stewart, M.G., Wang, S., Donelick, H.M., Tamayo-Jaramillo, D., Greer, D.L., Zhu, D., Li, W. and Shen, P.S., 2023. Lysate-to-grid: Rapid Isolation of Native Complexes from Budding Yeast for Cryo-EM Imaging. Bio-protocol, 13(2).
- Dillon, L.A., Okrah, K., Hughitt, V.K., Suresh, R., Li, Y., Fernandes, M.C., Belew, A.T., Corrada Bravo, H., Mosser, D.M. and El-Sayed, N.M., 2015. Transcriptomic profiling of gene expression and RNA processing during *Leishmania* major differentiation. Nucleic acids research, 43(14), pp.6799-6813.
- Graf, F.E., Ludin, P., Arquint, C., Schmidt, R.S., Schaub, N., Kunz Renggli, C., Munday, J.C., Krezdorn, J., Baker, N., Horn, D. and Balmer, O., 2016. Comparative genomics of drug resistance in *Trypanosoma brucei rhodesiense*. Cellular and molecular life sciences, 73, pp.3387-3400.
- Gutierrez Guarnizo, S.A., Tikhonova, E.B., Zabet-Moghaddam, M., Zhang, K., Muskus, C., Karamyshev, A.L. and Karamysheva, Z.N., 2021. Drug-Induced Lipid Remodeling in *Leishmania* Parasites. Microorganisms, 9(4), p.790.
- Kelley, L.A., Mezulis, S., Yates, C.M., Wass, M.N. and Sternberg, M.J., 2015. The Phyre2 web portal for protein modeling, prediction and analysis. Nature protocols, 10(6), pp.845-858.
- Kozakov, D., Hall, D.R., Xia, B., Porter, K.A., Padhorny, D., Yueh, C., Beglov, D. and Vajda, S., 2017. The ClusPro web server for protein-protein docking. Nature protocols, 12(2), pp.255-278.
- Liwo, A., Khalili, M., Czaplewski, C. and Kalinowski, S., 2007. Ołdziej, S., Wachucik, K., Scheraga, HA: Modification and optimization of the united-residue (UNRES) potential energy function for canonical simulations. I. Temperature dependence of the effective energy function and tests of the optimization method with single training proteins. Journal

of Physical Chemistry B, 111(1), pp.260-285.

Mirdita, M., Schütze, K., Moriwaki, Y., Heo, L., Ovchinnikov, S. and Steinegger, M., 2022. ColabFold: making protein folding accessible to all. Nature methods, 19(6), pp.679-682.

Mo, C. and Bard, M., 2005. A systematic study of yeast sterol biosynthetic protein–protein interactions using the split-ubiquitin system. Biochimica et Biophysica Acta (BBA)-Molecular and Cell Biology of Lipids, 1737(2-3), pp.152-160.

Mo, C., Valachovic, M. and Bard, M., 2004. The ERG28-encoded protein, Erg28p, interacts with both the sterol C-4 demethylation enzyme complex as well as the late biosynthetic protein, the C-24 sterol methyltransferase (Erg6p). Biochimica et Biophysica Acta (BBA)-Molecular and Cell Biology of Lipids, 1686(1-2), pp.30-36.

Mukherjee, S., Moitra, S., Xu, W., Hernandez, V. and Zhang, K., 2020. Sterol 14 α -demethylase is vital for mitochondrial functions and stress tolerance in Leishmania major. PLoS Pathogens, 16(8), p.e1008810.

Mwenechanya, R., Kovářová, J., Dickens, N.J., Mudaliar, M., Herzyk, P., Vincent, I.M., Weidt, S.K., Burgess, K.E., Burchmore, R.J., Pountain, A.W. and Smith, T.K., 2017. Sterol 14 α -demethylase mutation leads to amphotericin B resistance in Leishmania mexicana. PLoS neglected tropical diseases, 11(6), p.e0005649.

Negreira, G.H., Monsieurs, P., Imamura, H., Maes, I., Kuk, N., Yagoubat, A., Van den Broeck, F., Sterkers, Y., Dujardin, J.C. and

Domagalska, M.A., 2022. High throughput single-cell genome sequencing gives insights into the generation and evolution of mosaic aneuploidy in Leishmania donovani. Nucleic acids research, 50(1), pp.293-305.

Ramos, H., Valdivieso, E., Gamargo, M., Dagger, F. and Cohen, B.E., 1996. Amphotericin B kills unicellular leishmanias by forming aqueous pores permeable to small cations and anions. The Journal of membrane biology, 152, pp.65-75.

t'Kindt, R., Scheltema, R.A., Jankevics, A., Brunker, K., Rijal, S., Dujardin, J.C., Breitling, R., Watson, D.G., Coombs, G.H. and Decuyper, S., 2010. Metabolomics to unveil and understand phenotypic diversity between pathogen populations. PLoS neglected tropical diseases, 4(11), p.e904.

Vijayakumar, S. and Das, P., 2019. Structural, molecular motions, and free-energy landscape of Leishmania sterol-14 α -demethylase wild type and drug resistant mutant: A comparative molecular dynamics study. Journal of Biomolecular Structure and Dynamics, 37(6), pp.1477-1493.

Vincent, I.M. and Barrett, M.P., 2015. Metabolomic-based strategies for anti-parasite drug discovery. Journal of biomolecular screening, 20(1), pp.44-55.

Waterhouse, A., Bertoni, M., Bienert, S., Studer, G., Tauriello, G., Gumienny, R., Heer, F.T., de Beer, T.A.P., Remper, C., Bordoli, L. and Lepore, R., 2018. SWISS-MODEL: homology modelling of protein structures and complexes. Nucleic acids research, 46(W1), pp.W296-W303.